

Hydrogen Chloride Removal from Flue Gas by Low-Temperature Reaction with Calcium Hydroxide

SUPPORTING INFORMATION

Revised Version

Alessandro Dal Pozzo, Raffaella Moricone, Giacomo Antonioni,

Alessandro Tugnoli, Valerio Cozzani

LISES – Dipartimento di Ingegneria Civile, Chimica, Ambientale e dei Materiali
Alma Mater Studiorum - Università di Bologna, via Terracini n.28, 40131 Bologna, Italy

S1. DETAILS ON EXPERIMENTAL SECTION

Materials

The solid reactant was calcium hydroxide, ACS reagent grade, supplied by Sigma Aldrich. The material was composed of 96% calcium hydroxide, $\text{Ca}(\text{OH})_2$, with the balance being calcium carbonate, CaCO_3 , as stated by the supplier. To prevent further carbonation of the samples due to contact with ambient air, the material was kept in HDPE sealed containers, placed in a ventilated cabinet. In order to restrict the natural variability of the material, the hydrated lime was sieved and only the fraction composed by particles between 45 and 123 μm of diameter was used in the experimental runs. The specific surface area of the sieved samples, as determined by nitrogen porosimetry (Micromeritics, Flow Sorb II 2300), was 15.1 m^2/g . Porosity and pore size distribution (see porosigram in section S3 of this Supporting Information) were determined by mercury intrusion porosimetry (Carlo Erba Strumentazione, Porosimeter 2000).

Quartz sand was used as inert filling material in the sorbent bed, in order to reduce the tendency of calcium hydroxide to form agglomerates and to minimize gas channelling.¹ A fraction of the same range of diameters as calcium hydroxide (45-123 μm) was used and preliminary runs performed by flowing the gas mixture through the reactor with and without a bed of only quartz sand showed no HCl sorption, thus confirming the material as inert.

FBR Runs – Apparatus

The experimental runs listed in Table 1 of the paper took place in a borosilicate glass tubular reactor cylinder 150 mm long by 15 mm of inner diameter, as shown in Figure S1. In the reactor, a layer of sorbent was deposited on a sintered glass frit disk positioned at 20 mm from the outlet section. The reactor simulates the conditions of a cake of particles deposited on the filter bags of a fabric filter: in

particular, the inner diameter was designed to have a superficial velocity of the flue gas of 0.9 m/min at 180 °C, corresponding to a typical design value for baghouses.² In order to operate at a constant temperature, the reactor was positioned in an oven with forced convection (Binder, FD-53).

The gas mixture containing HCl was prepared diluting the stream coming from a cylinder of HCl at 3% in nitrogen with a stream of dry nitrogen. Mass flow controllers (Bronkhorst, EL-FLOW) operating in the range 0.4-20 NmL/min were used to obtain the desired HCl concentration. Gas lines and tube fittings made of PTFE and glass 3-way stopcocks and cross connectors were used to feed the gas stream to the reactor.

A Fourier transform infrared (FTIR) spectrometer was used for the quantitative characterization of HCl concentration in the gas stream. A Bruker TENSOR 27 device equipped with a MCT detector and a specifically developed low volume gas cell (8.7 mL) with a 123mm pathlength was used. The gas cell, with internal windows of ZnSe, was heated at a constant temperature of 200 °C, in order to prevent adsorption of HCl on the internal surface of the cell. The reactor was connected to the FTIR spectrometer using a transfer line with a 2 mm internal diameter PTFE tube. A line bypassing the FBR allows the gas stream to be fed directly to the FTIR both before the start and at the end of the reaction runs, in order to verify the inlet gas composition. The gas leaving the FTIR was disposed by a soda bath and sent to a hood.

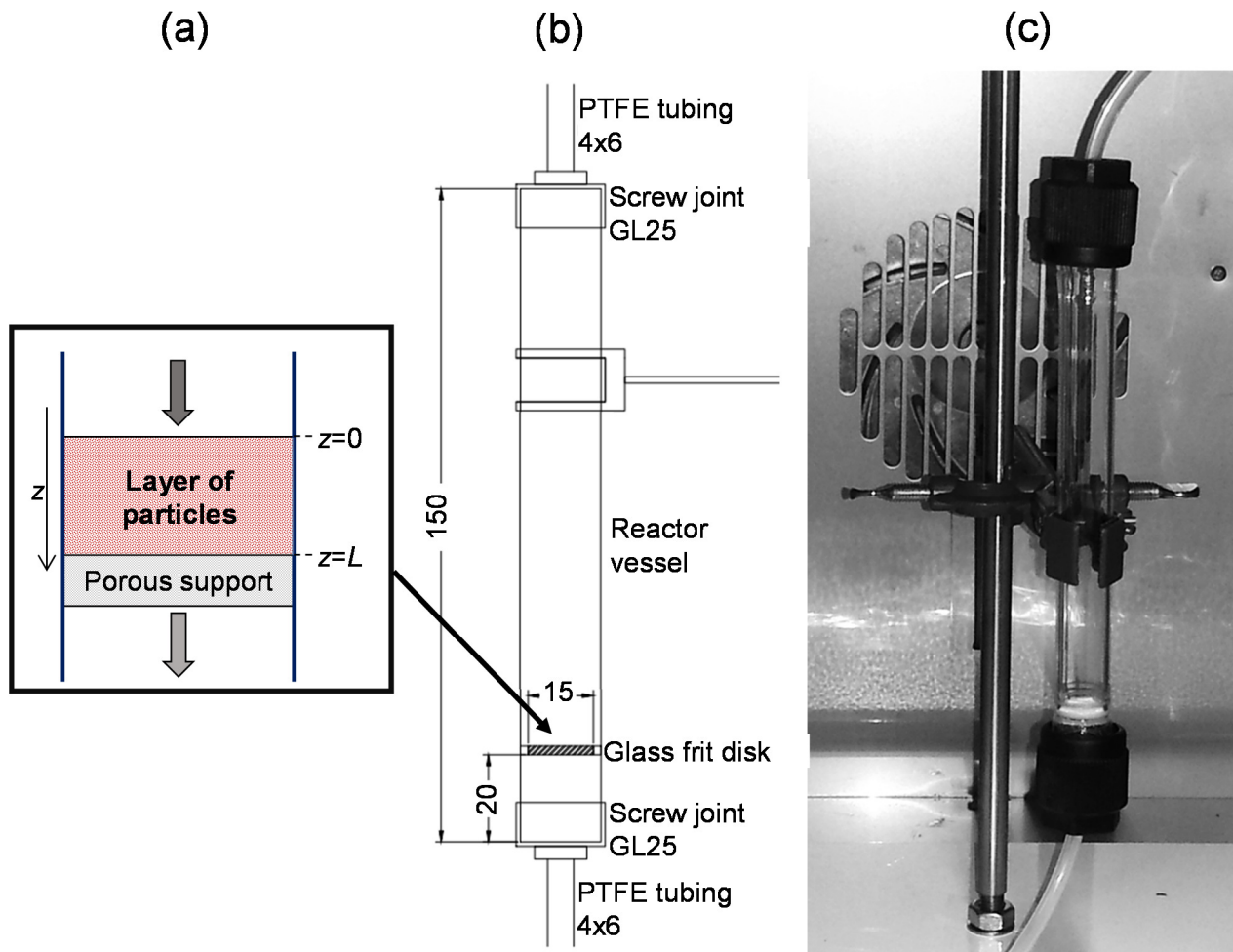


Figure S1. Detail of the tubular reactor: a) sketch of the reacting system; b) sketch and c) picture of the reactor.

FBR Runs – Procedure

The experimental protocol followed for the FBR runs was the following. Before each experimental run, the sorbent and inert material were introduced in the reactor, taking care of forming an even layer of particles. Approximate thickness of the layer was 1.6-2.2 mm depending on the mass of sorbent. A nitrogen purge flow (180 NmL/min for at least 30 min) was started to condition the fixed bed, while heating the oven to the desired temperature. Then, the flow gas composition was changed to that required for the run and was sent to the FTIR by the bypass line in order to check the HCl concentration. The gas

flow was then switched to the reactor line, until the recorded FTIR spectra showed a complete breakthrough of the reaction bed. When this condition was detected, the gas flow was diverted to the bypass line to check that no differences were present with respect to the recorded intensity of HCl concentration. If this check was verified, the run was stopped, allowing the system to cool down while purging the reactor with dry nitrogen.

The FTIR spectra were recorded between 8000 and 400 cm^{-1} , at a resolution of 4 cm^{-1} . Each spectrum recorded is obtained as average of 16 consecutive scans. This resulted in a time resolution of 3.7 s.

The FTIR spectra were recorded and elaborated using the Bruker OPUS/IR software. The profile of HCl and of H_2O in the outlet gas and the total amount reacted were obtained assessing the integrated absorbance as a function of time on the characteristic wavenumber intervals: for HCl, the absorption band between 3150 and 2500 cm^{-1} was considered, corresponding to roto-vibrational transitions of HCl in the gas phase;³ for water vapour, the interval between 4000 and 3500 cm^{-1} was used.

Integrated absorbance values were correlated to the concentration in the gas by the Lambert-Beer law, which can be expressed over a characteristic wavenumber interval as follows:

$$I = \int_{\nu_1}^{\nu_2} A(\nu) \cdot d\nu = \int_{\nu_1}^{\nu_2} \varepsilon(\nu) \cdot l \cdot C \cdot d\nu = K \cdot C \quad (\text{S1})$$

where I is the integral absorbance value, A the measured spectral absorbance, ε the extinction coefficient of the gaseous compound, l the optical length used in the measurement, C the concentration, and (ν_1, ν_2) the wavenumber interval selected for the measurement. The calibration constant, K , may be considered independent of the concentration if deviations from the Lambert-Beer linear correlation can be neglected, as in the range of HCl concentrations considered. The value of K for HCl was obtained from experimental calibration using gas mixtures of known composition, following the procedure described by Bak and Larsen.⁴ No quantitative calibration was carried out for water.

The conversion of the solid reactant X_s was calculated cumulatively from the registered data on HCl removal as follows:

$$\chi_s = \frac{b}{n_s} \int_0^{t_{fin}} Q \cdot C_{in} \left(1 - \frac{C_{out}}{C_{in}}\right) dt \quad (S2)$$

where b is the stoichiometric coefficient of the sorbent (1 if the product is CaOHCl, 0.5 if the product is CaCl₂), n_s the moles of sorbent initially charged in the reactor, Q the flow rate of the gas mixture, C_{in} and C_{out} respectively the inlet and outlet molar concentration of HCl in the gas.

Thermogravimetry (TGA)

A TGA-Q500 thermogravimetric analyzer from TA Instruments-Water (USA) was used to characterize the sorbent materials before and after the reaction. Thermogravimetric (TG) analysis was performed on samples of about 20 mg of sample. The thermal program applied in experimental runs consisted in a drying step (isotherm at 105°C for 10 minutes) followed by a temperature ramp at constant heating rate (10°C/min) up to the final temperature of 800°C, under a purge gas flow of pure nitrogen (60 mL/min). TG runs were repeated at least 3 times, obtaining a variance of the reported results below 2%.

TG-FTIR Analysis

Simultaneous TG-FTIR measurements for the online analysis of evolved gases formed during the thermal decomposition of solid samples after reaction were carried out coupling a FTIR spectrometer (Bruker Equinox 55, equipped with MCT detector and a gas cell identical to that described in section 2.1) to a Netzsch STA 409/C thermoanalyzer using a heated PTFE transfer line to avoid the condensation of decomposition products. TG runs were carried out under a pure N₂ purge flow (60 mL/min) at a constant heating rate of 20 °C/min. The gas flow from the TG outlet to the IR gas cell was of 60 mL/min. A residence time of 30 s in the transfer line was assessed and assumed as the time delay correction between

TG and IR results. The temporal resolution of IR spectra collection was of 9.7 s, more than sufficient to follow the gas evolution rates characteristic of TG runs at the adopted heating rate.⁵ The wavenumber intervals used to extract the emission profiles for the different gas species were the following: 4025-3792 cm^{-1} for H_2O , 2971-2952 cm^{-1} for HCl , 2400-2240 cm^{-1} for CO_2 .

X-ray Diffractometry

Phase identification in the solid samples after reaction was performed by X-ray diffractometry. The diffractometer (PANalytical Empyrean) was operated at 40 kV and 30 mA using Cu K_α radiation. In order to complement the TG-FTIR analysis on solid residues, the sample was placed in an Anton-Parr XRK 900 high-temperature reactor chamber and XRD spectra collection was performed at temperatures up to 700 °C. The chamber was heated at a rate of 20 °C/min to reach each measurement temperature. Then, after 5 min, the sample was scanned over a 2θ range of 20-80° using a step size of 0.0275° per second.

S2. DETAILS ON MODELLING

A brief discussion about the required set of geometrical, morphological and thermodynamic input data and the assumptions introduced to apply the model to the specific geometry used in FBR runs is reported in the following. Pore size distribution of the sorbent sample was used to determine the initial size of sorbent grains. The method of Heesink et al.⁴⁴ was applied to the purpose, as described in section S3 of the SI. Three temperature-dependent model parameters need to be determined by experimental data fitting: k_s , the chemical reaction rate constant (m/s), D_s , the product layer diffusivity of the gaseous reactant (m²/s) and K , the non-dimensional numerical coefficient determining the mechanical work associated to nucleation of solid reaction product. A sensitivity analysis was carried out to determine the effect of variations in the fitting parameters on model results, applying the variance-based method,⁴⁵ as described in section S4 of the SI.

Modelling of the Packed Bed

In the experimental configuration, acid gas removal takes place in a fixed bed of porous particles of thickness L , through which the gaseous phase flows at a constant velocity u_0 , mixing axially according to a dispersion coefficient D_z . Thus, a one-dimensional mass balance differential equation with convection, axial diffusion and reaction through a porous medium can be applied:

$$\varepsilon \cdot \frac{\partial C}{\partial t} = -u_0 \cdot \frac{\partial C}{\partial z} + \varepsilon \cdot D_z \cdot \frac{\partial^2 C}{\partial z^2} - r_{vb} \quad (\text{S3})$$

with the following initial and boundary conditions:

$$C(z, t = 0) = 0$$

$$C(z = 0, t) = C_0$$

$$\left. \frac{\partial C}{\partial z} \right|_{z=L} = 0$$

where C is the bulk concentration of reactant gas, ε is the interparticle void fraction of the packed bed, r_{vb} is the reaction rate for a unit volume of bed and C_0 is the concentration of the reactant gas at the entrance of the bed ($z = 0$).

The reaction term r_{vb} can be expressed as follows:

$$r_{vb} = k_o \cdot (C - C_{eq}) \quad (\text{S4})$$

where C_{eq} is the minimum theoretical concentration that would be reached at thermodynamic equilibrium and k_o is an overall reaction rate constant (expressed in s^{-1}).

Modelling of the gas-solid reaction

In order to derive an expression for k_o , the fundamental model detailed in Antonioni et al.⁶ was applied. This approach integrates the conventional grain model⁷ with a crystallization and fracture (CF) submodel⁸ for the sake of accurately describing the decline in reactivity of the sorbent during the process:

- i) as in the typical grain model framework, sorbent particles are made of non-porous spherical grains and a void fraction. Grains are the reacting entities and their size distribution in grain classes can be obtained from measurable characteristics of the sorbent, as described in section S3. The chloridation of $\text{Ca}(\text{OH})_2$ grains is a gas-solid reaction with generation of a solid product, thus controlled by chemical reaction rate (k_s) and product layer diffusivity (D_s).
- ii) the CF submodel introduces a reduction factor RF of reaction velocity in order to take into account the increasing mechanical hindrance to product nucleation generated by the growing product layer over time. The relationships that bring to the determination of RF are listed in Table S1 and fully explained elsewhere.⁶

The resulting expression for k_o is the sum of the reactivity of the grain classes, weighted by their volume fraction v_i and reduced by their respective RF_i :

$$k_o = \sum_i \left[v_i \cdot RF_i \cdot \frac{3 \cdot (1 - \varepsilon) \cdot (1 - \omega_{in}) \cdot (1 - \varepsilon_p) \cdot r_{c,i}^2}{r_{g,i}^3} \cdot \frac{D_s \cdot k_s}{D_s + k_s \cdot r_{c,i} \cdot \left(1 - r_{c,i}/r_{t,i}\right)} \right] \quad (S5)$$

Explanation of symbols used in eq. (S5) is reported in the nomenclature section.

Eventually, the conversion of the sorbent is obtained as a weighted summation of the conversion of the grain classes i , which is a function of the shrinking of the unreacted grain core.⁶

Table S1. Equations of the nucleation submodel for each grain class i .

Reduction factor	$RF = \frac{PNC(C_{HCl}, h) \cdot r_k(C_{HCl}, h)^2}{PNC(C_{HCl}, 0) \cdot r_{k,0}(C_{HCl}, 0)^2}$
Population of nuclei of critical size	$PNC = 4\pi r_c^2 \zeta \cdot \exp\left(-\frac{\Delta G(r_k)}{k_b T}\right)$
Radius of a critical nucleus	$r_k = -\frac{\sigma}{\rho_m \Delta G_c} \left(1 + \sqrt{1 - \frac{\rho_m \Delta G_c}{\sigma} M_W h^{\frac{3}{2}}} \right)$
Overall free energy change associated with the formation of a nucleus of radius r	$\begin{aligned} \Delta G(r) &= \Delta G_{surface}(r) + \Delta G_{volume}(r) + W(r) \\ &= 4\pi r^2 \sigma + \frac{4}{3} \pi r^3 \rho_m \Delta G_c + M_W 4\pi r \sigma h^{\frac{3}{2}} \end{aligned}$
Lumped work-related parameter M_W	$M_W = \frac{K(1 - 1/\alpha)^{\frac{1}{3}} (1 - \varepsilon_{pl})^4}{d^{\frac{1}{2}}}$

Model Parameters

The geometrical, thermodynamic and mass transfer parameters required by the model, as well as the values assumed in the present application, are reported in Table S2. Pore size distribution of the sorbent

sample is used to determine the initial size of sorbent grains. The method of Heesink et al.⁹ was applied to the purpose, as described in section S3.

Three model parameters remain to be determined by experimental data fitting: k_s , the chemical reaction rate constant (m/s), D_s , the product layer diffusivity of the gaseous reactant (m²/s) and K , the non-dimensional numerical coefficient in the expression of M_w . Arrhenius-type law was assumed for the temperature dependence of k_s and D_s , being both thermally-activated processes (Bhatia and Perlmutter, 1982), while a log-linear decrease with temperature was considered for the mechanical work constant K (the elastic modulus of metal oxides and hydroxides shows exponential decay with temperature).⁶

Therefore, the three parameters can be expressed as:

$$par(T) = A \cdot \exp\left(\frac{E_A}{RT}\right) \quad (S3)$$

where A (same unit of measurement as the parameter) is an apparent pre-exponential coefficient and E_A (J/mol) the activation energy. These are the coefficients to be directly estimated, in order to obtain the slopes of temperature dependence for k_s , D_s and K that best fit the data. The adopted procedure, based on the least square method, is discussed in Antonioni et al.⁶

Table S2. Summary of input parameters required for the model and values calculated, assumed or experimentally determined for model application in the present study.

Type	Item	Description / Definition	Value	Units	Source
<i>Geometrical parameters</i>	ε	Inter-particle void fraction of the fixed bed	0.42	-	Result of mercury porosimetry
	ω_m	Volumetric fraction of inert material in the bed	0.68-0.81	-	Inert-to-sorbent ratio in Table 1
	ε_p	Intra-particle void fraction (porosity)	0.30	-	Result of mercury porosimetry
	ε_{pl}	Void fraction of the product layer	0.26	-	Hexagonal packing
	S_{BET}	Specific surface area	15.1	m ² /g	Result of nitrogen porosimetry
	α	Volumetric expansion factor, i.e. ratio of the molar volume of the solid product to that of the solid reactant: $\alpha = V_{m,p} / V_{m,s}$	1.58	-	10
<i>Thermodynamic parameters</i>	C_{eq}	Equilibrium concentration of the gaseous reactant	3.42×10^{-7} (a)	mol/m ³	11
	ΔG^0	Standard molar free energy change of the reaction	-6.75×10^4 (a)	J/mol	
	σ	Surface energy per unit area of the solid product	0.25	J/m ²	6
<i>Mass transfer parameters</i>	D_m	Molecular diffusivity of the gaseous reactant	3.66×10^{-5} (a)	m ² /s	Fuller-Schettler-Giddings correlation ¹²
	D_z	Axial dispersion coefficient	$0.7 \cdot D_m$	m ² /s	13

(a) values for $T = 180$ °C

S3. GRAIN SIZE DISTRIBUTION FROM POROSIMETRY DATA

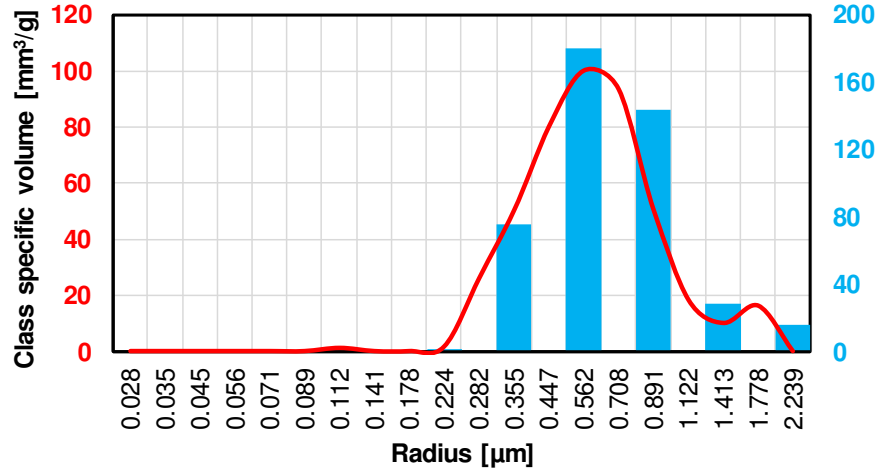


Figure S2. Mercury porosigram of the hydrated lime adopted in the study and division of the pore volume in 8 pore classes.

In the classical grain model approach, the reacting unit of sorbent is the grain and it is assumed that all the grains share the same initial radius r_g .¹⁴ This value is calculated assuming that the sum of the surface of the grains in a single, unreacted particle corresponds to the specific surface area S_{BET} of the sorbent:

$$r_g = \frac{3}{\rho_s \cdot S_{BET}} \quad (\text{S6})$$

where ρ_s is the true density of the solid.

In order to take into account the pore distribution of the material, the hypothesis of uniform grains can be overcome by introducing grain classes according to the method of Heesink et al.⁹

The size distribution of pores is obtained by means of mercury intrusion porosimetry and the pores of the sample are divided in a set of size classes (e.g. 8 classes, Figure S2). Each class i has a mean pore radius $r_{pore,i}$ and an associated initial grain radius $r_{g,i}$ such as:

$$r_{g,i} = F \cdot r_{pore,i} \quad (\text{S7})$$

The proportionality factor F between corresponding pore and grain radius is called the pore-to-sphere factor and is given by:

$$F = \frac{3}{\rho_s \cdot S_{BET}} \sum_i \frac{v_i}{r_{pore,i}} \quad (S8)$$

where v_i is the fraction of grains belonging to size class i and is equal to the ratio of the volume of the corresponding pore class to the total pore volume of the material.

For the present study, the value of F is 0.164. Computed grain radius for the 8 class subdivision of Figure S2 are reported in Table S3.

Table S3. Division of the pore size distribution in Figure S1 in pore classes and related grain sizes.

Pore class	Average class radius μm	Cumulative pore volume mm^3/g	Class specific volume		$r_{g,i}$ m
			mm^3/g	%	
1	2.239	16.1	16.1	3.6%	3.67E-07
2	1.413	44.4	28.3	6.3%	2.32E-07
3	0.891	188.3	143.9	32.2%	1.46E-07
4	0.562	368.3	180.0	40.2%	9.23E-08
5	0.355	444.4	76.1	17.0%	5.82E-08
6	0.224	446.1	1.7	0.4%	3.67E-08
7	0.141	447.2	1.1	0.2%	2.32E-08
8	0.089	447.2	0.0	0.0%	1.46E-08

S4. DETAILS ON SENSITIVITY ANALYSIS

A sensitivity analysis was carried out to determine the effect of variations in the fitting parameters (k_s , D_s , K) on model results, applying the variance-based method.¹⁴

Any model output Y can be considered a function of input factors (X_1 to X_k), in the general form:

$$Y = f(X_1, X_2, \dots, X_k) \quad (\text{S9})$$

The unconditional variance of the model output $V(Y)$ can be expressed by means of k first-order effect indices S_i , or main effect indices, which measure the effect of varying a single input X_i on Y , and k total effect indices (S_{Ti}), taking into account the uncertainty caused by the interaction of an input factor with any other input variable. The first-order sensitivity index is defined as follows:

$$S_i = \frac{V_{X_i} \left(E_{X_{\sim i}}(Y|X_i) \right)}{V(Y)} \quad (\text{S10})$$

where the numerator represents the first-order effect of X_i on Y (the meaning of the symbols is reported in nomenclature). Therefore, the index can be interpreted as a measure of the variance reduction that would be achieved fixing X_i . Since V_{X_i} varies between zero and $V(Y)$, S_i is a normalized index and the summation of all first-order indices is equal to 1 at most. The total effect index S_{Ti} takes into account first and higher order effects (i.e. interactions of factor X_i) and is defined as follows:

$$S_{Ti} = \frac{E_{X_{\sim i}} \left(V_{X_i}(Y|\mathbf{X}_{\sim i}) \right)}{V(Y)} = 1 - \frac{V_{X_{\sim i}} \left(E_{X_i}(Y|\mathbf{X}_{\sim i}) \right)}{V(Y)} \quad (\text{S11})$$

The index captures the contribution of all terms in the variance decomposition which include X_i . In this case, their summation can be higher than 1, since e.g. the effect of the interaction between X_i and X_j is taken into account in both S_{Ti} and S_{Tj} .

The assessment of the variance indexes as a function of the input factors was obtained by means of the estimators proposed by Saltelli et al.¹⁴ The procedure is based on the assumption of independence of input factors, which have to be uniformly distributed in the range 0-1. The first step consists in the

creation of the $2+k$ matrices (\mathbf{A} , \mathbf{B} , and $\mathbf{A}_B^{(i)}$) each one containing N sample sequences. This is the best triplet available to optimise the computational efficiency when a quasi-random (QR) sequence is used to create the sample points. QR sequences are designed to generate samples as uniform as possible, taking into account the position of previously points and filling corresponding gaps. In the present work, Sobol QR sequence has been adopted to generate the sample matrices.

Once computed the sample matrices, they were used to calculate the estimators required for the assessment of the sensitivity indices. The formula for calculating S_i , defined in Eq. (S10), is the following:

$$V_{X_i} \left(E_{X_{\sim i}}(Y|X_i) \right) = \frac{1}{N} \sum_{j=1}^N \left(f(\mathbf{B})_j \cdot \left(f(\mathbf{A}_B^{(i)})_j - f(\mathbf{A})_j \right) \right) \quad (\text{S12})$$

In order to compute S_{Ti} , shown in Eq. (S11), the estimator originally proposed by Jansen¹⁵ was chosen:

$$E_{X_{\sim i}} \left(V_{X_i}(Y|X_{\sim i}) \right) = \frac{1}{2N} \sum_{j=1}^N \left(f(\mathbf{A})_j - f(\mathbf{A}_B^{(i)})_j \right)^2 \quad (\text{S13})$$

In Sobol sequence, the sample points are added sequentially, permitting to determine their number (N) when the values of the indices reach a suitable convergence. Here, $N = 5000$ was adopted, following the recommendation by Saltelli et al.¹⁴

The denominator of both indices is the unconditional variance of the output $V(Y)$, which was calculated as the expected value of the squared deviation from the unconditional mean $E(Y)$:

$$V(Y) = E([Y - E(Y)]^2) \quad (\text{S14})$$

S5. HCL REMOVAL EFFICIENCY DURING FBR RUNS

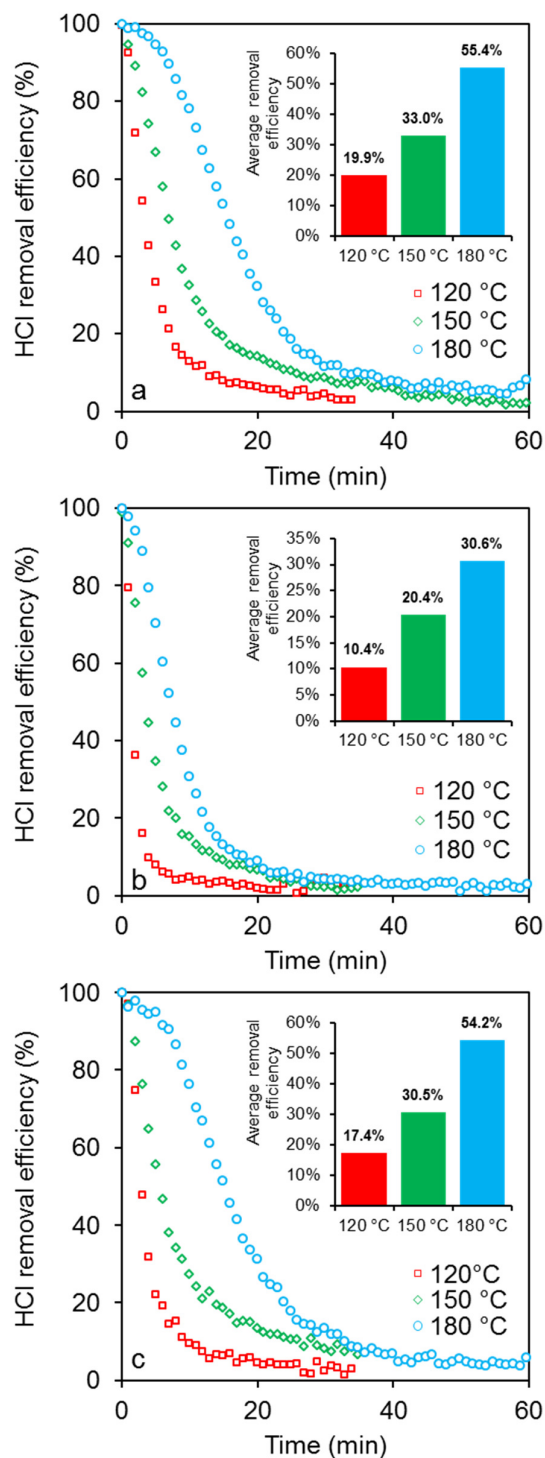


Figure S3. Profile of HCl removal efficiency over time for the runs at (a) 2500 ppm HCl and 100 mg Ca(OH)₂, (b) 2500 ppm HCl and 50 mg Ca(OH)₂, (c) 1250 ppm HCl and 50 mg Ca(OH)₂. Inset: average HCl removal efficiency obtained during the first 30 min of experiment.

S6. COMPLEMENTARY THERMOGRAVIMETRIC ANALYSIS OF SOLID RESIDUES

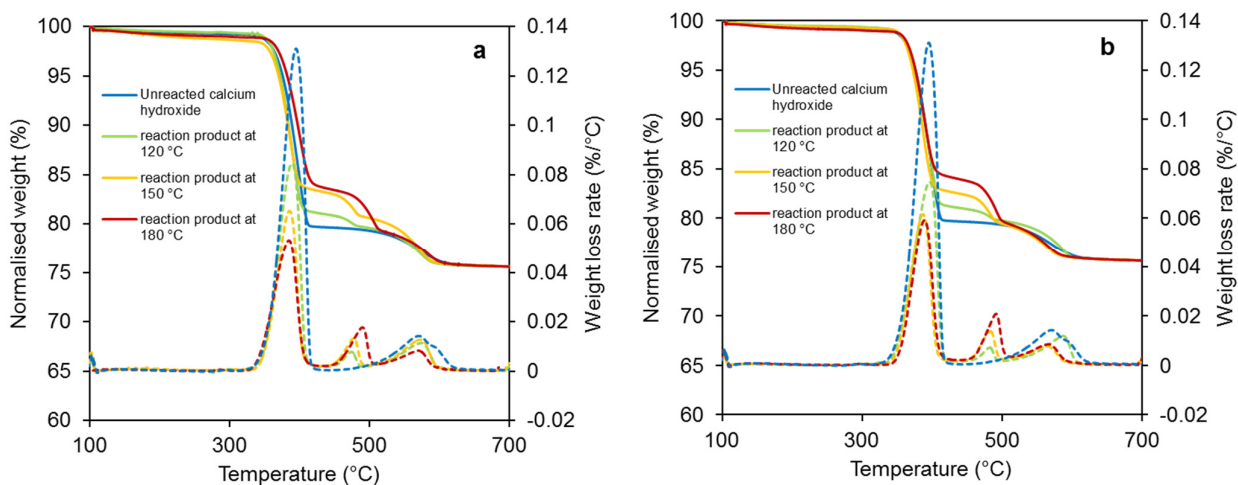


Figure S4. Weight loss (solid curves) and weight loss rate (dotted curves) for unreacted $\text{Ca}(\text{OH})_2$ and solid residues obtained from the FBR after runs at temperatures of 120, 150 and 180 °C, for the cases with 2500 ppm of HCl and 50 mg of sorbent (panel a) and with 1250 ppm of HCl and 50 mg of sorbent (panel b). TG runs were carried out at 10 °C/min constant heating rate and in 100 mL/min pure nitrogen flow. Weight loss of the reacted samples is rescaled and normalized to the one of unreacted $\text{Ca}(\text{OH})_2$, in order to subtract the presence of inert material in the sample collected after FBR runs.

S7. XRD ANALYSIS

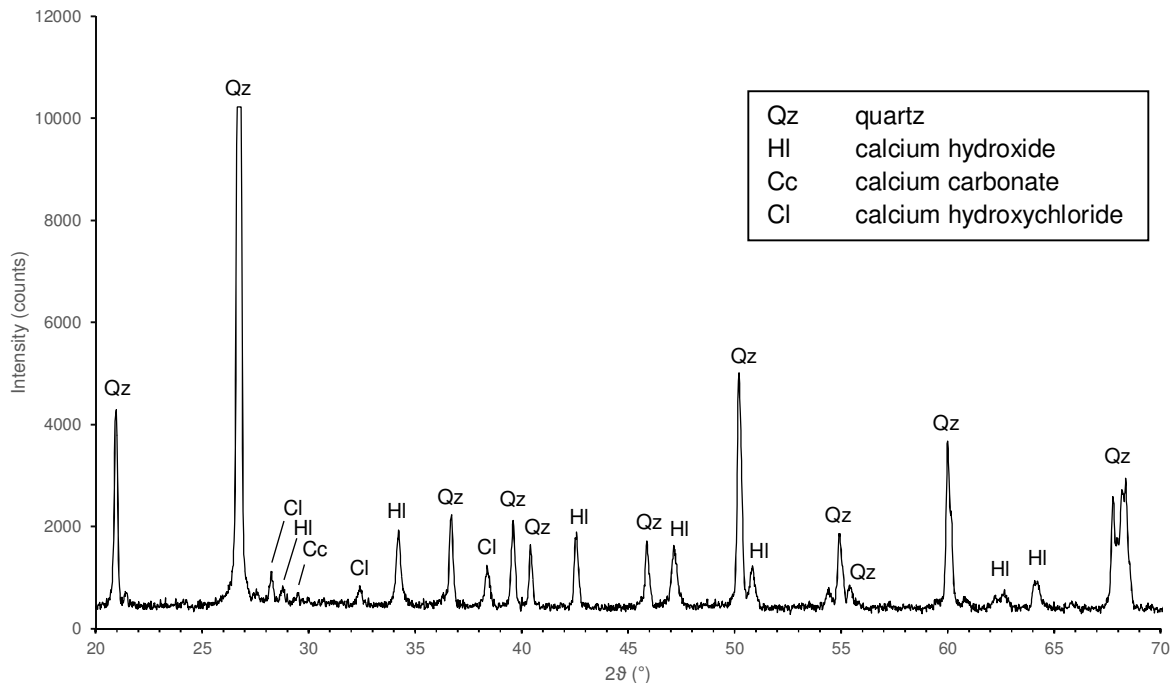


Figure S5. XRD spectrum of a sample (inert + calcium hydroxide, 3:1 ratio) reacted with HCl (2500 ppm) at 180 °C.

Table S4. PDF card and 2-theta positions of the main peaks of the compounds of interest for XRD phase identification.

Compound	PDF no.	2-theta locations (°)
Ca(OH) ₂ , portlandite	04-0733i	18.1, 28.7, 34.1 , 47.1, 50.8, 54.3
CaOHCl, calcium hydroxide chloride	36-0883i	28.1, 32.3, 38.3 , 47.0
CaCl ₂ , calcium chloride	24-0233	19.8, 29.3 , 31.2, 38.6
CaCO ₃ , calcite	05-0586	23.0, 29.4 , 36.0, 40.0, 47.5, 48.5

S8. PARAMETERS OBTAINED BY EXPERIMENTAL DATA FITTING

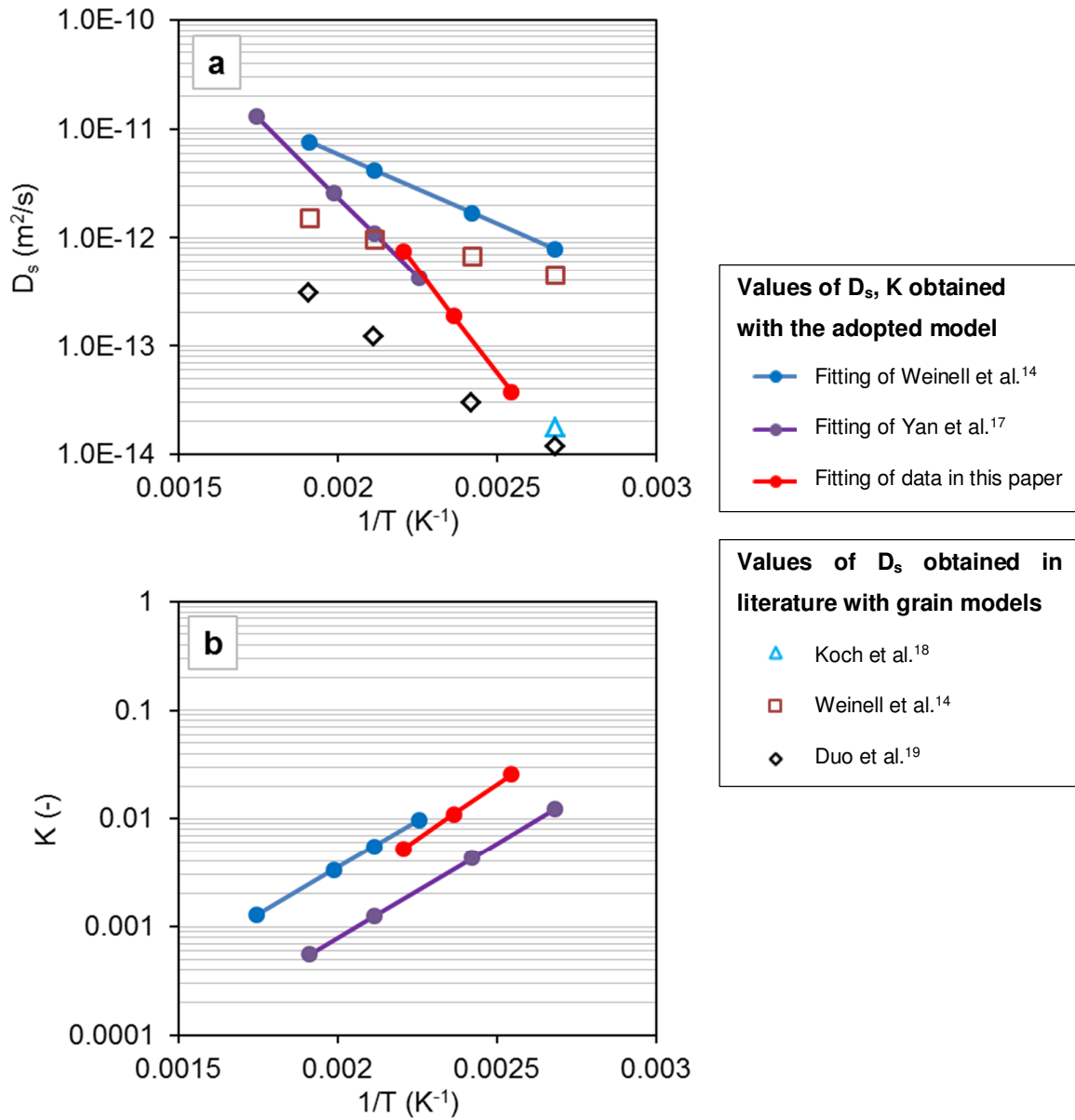


Figure S6. (a) Product layer diffusivity during reaction between $Ca(OH)_2$ and HCl estimated for the training set of experimental runs in this paper, compared to values obtained in previous applications of the adopted model and to values obtained by different studies which modelled the chloridation reaction in similar conditions with grain models. (b) Numerical coefficient K estimated for the training set of experimental runs in this paper, compared to values obtained in previous applications of the adopted model.

NOMENCLATURE

In the modelling section

C_0	gas concentration entering the bed (mol/m ³)
C_{eq}	equilibrium concentration (mol/m ³)
d	average diameter of product layer crystallites (m)
D_m	molecular gas diffusivity (m ² /s)
D_z	axial dispersion coefficient (m ² /s)
E_A	activation energy (J/mol)
F	pore-to-sphere ratio
h	thickness of the product layer (m)
K	non-dimensional numerical coefficient (-)
k_b	Boltzmann constant (m ² ·kg·s ⁻² ·K ⁻¹)
k_s	reaction rate constant per unit area (m/s)
L	thickness of the sorbent bed (m)
PNC	population of nuclei of critical size (-)
r_c	radius of the unreacted core of a grain (m)
RF	reduction factor introduced with the nucleation submodel (-)
r_g	initial grain radius (m)
r_k	radius of a critical nucleus of product (m)
r_t	total radius of a grain (m)
r_{vb}	reaction rate per unit volume of the bed (mol·m ⁻³ ·s ⁻¹)
S_{BET}	BET surface area of the sorbent (m ² /kg)
u_0	gas velocity (m/s)
\dot{V}	gas flow rate (m ³ /s)
V_c	volume of the unreacted core of a grain (m ³)
$V_{m,s}$	molar volume of the sorbent (m ³ /mol)
$V_{m,p}$	molar volume of the solid product (m ³ /mol)

W	mechanical work required for product layer growth (J)
ΔG	total free energy change (J)
ΔG^0	standard molar free energy change of the reaction (J/mol)

Greek Letters

α	ratio between the molar volume of solid reactant and of solid product (-)
ε	void fraction of the bed (-)
ε_p	porosity of a sorbent particle (-)
ε_{pl}	porosity of the product layer (-)
ζ	number of molecules of solid reactant per unit area of reaction interface (m^{-2})
v_i	fraction of grains belonging to size class i
ρ_b	bulk density of the sorbent (kg/m^3)
ρ_m	molar density of product (mol/m^3)
ρ_s	true density of the sorbent (kg/m^3)
σ	surface energy per unit area of the product (J/m^2)
ω_{in}	fraction of inert material in the bed (-)

In the sensitivity section

k	number of uncertain input factors
N	number of sample points
i	index from 1 to k
j	index from 1 to N
X_i	generic uncertain input factor, with $X_i \in [0, 1]$
x_{ji}	generic value for factor X_i taken from row j of X_i
Y	generic scalar model output equal to $Y = f(X_1, X_2, \dots, X_k)$
X	$N \times k$ matrix of input factors
X_{-i}	$N \times (k - 1)$ matrix of all factors but X_i
A, B	$N \times k$ independent sample matrices with a_{ji} and b_{ji} as generic elements

$A_B^{(i)}$ matrix, where column i comes from matrix B and all other $k-1$ columns come from matrix A

$V_b(a)$ variance of argument a taken over b

$E_b(a)$ expected value of argument a taken over b

REFERENCES IN SUPPORTING INFORMATION

- (1) Chisholm, P.N.; Rochelle, G.T. Dry absorption of HCl and SO₂ with hydrated lime from humidified flue gas. *Ind. Eng. Chem. Res.* **1999**, 38, 4068-4080.
- (2) Green, D.; Perry, R. *Perry's Chemical Engineers' Handbook*; 8th edition, McGraw-Hill: New York, NY (USA), **2007**.
- (3) Tipler, P. A.; Llewellyn, R.A. *Modern Physics*; W. H. Freeman & Co.: New York, NY (USA), **2012**.
- (4) Bak, J.; Larsen, A. Quantitative gas analysis with FT-IR: a method for CO calibration using partial least-squares with linearized data. *Appl. Spectrosc.* **1995**, 49, 437-443.
- (5) Barontini, F.; Marsanich, K.; Cozzani, V. The use of TG-FTIR technique for the assessment of hydrogen bromide emissions in the combustion of BFRs. *J. Therm. Anal. Calorim.* **2004**, 78, 599-619.
- (6) Antonioni, G.; Dal Pozzo, A.; Guglielmi, D.; Tugnoli, A.; Cozzani, V. Enhanced modelling of heterogeneous gas-solid reactions in acid gas removal dry processes. *Chem. Eng. Sci.* **2016**, 148, 140-154.
- (7) Szekely, J.; Evans, J.W.; Sohn, H.Y. *Gas-Solid Reactions*; Academic Press: London (UK), **1976**.
- (8) Duo, W.; Seville, J.P.K.; Kirkby, N.F.; Clift, R., 1994. Formation of product layers in solid-gas reactions for removal of acid gases. *Chem. Eng. Sci.* **1994**, 49, 4429-4442.
- (9) Heesink, A.B.M.; Prins, W.; van Swaaij, W.P.M. A grain size distribution model for non-catalytic gas-solid reactions. *Chem. Eng. J.* **1993**, 53, 25-37.
- (10) NIST, NIST Chemistry WebBook. Available at: <http://webbook.nist.gov/chemistry/> (last accessed: 19/09/2017).
- (11) NIST, JANAF Thermochemical Tables. Available at: <http://kinetics.nist.gov/janaf/> (last accessed: 19/09/2017).

- (12) Fogler, H. S. *Elements of chemical reaction engineering*; Prentice Hall: Upper Saddle River, NJ (USA), **2005**.
- (13) Harker, J.H.; Backhurst, J.R.; Richardson, J.F. *Coulson and Richardson's Chemical Engineering: Volume 2 - Particle Technology and Separation Processes*; 5th edition, Butterworth-Heinemann: Oxford (UK), **2002**.
- (14) Weinell, C.E.; Jensen, P.I.; Dam-Johansen, K.; Livbjerg, H. Hydrogen chloride reaction with lime and limestone: kinetics and sorption capacity. *Ind. Eng. Chem. Res.* **1992**, 31, 164-171.
- (15) Saltelli, A.; Annoni, P.; Azzini, I.; Campolongo, F.; Ratto, M.; Tarantola, S. Variance based sensitivity analysis of model output. Design and estimator for the total sensitivity index. *Comput. Phys. Commun.* **2010**, 181, 259-270.
- (16) Jansen, M.J.W. Analysis of variance designs for model output. *Comput. Phys. Commun.* **1999**, 117, 35-43.
- (17) Yan, R.; Chin, T.; Tee Liang, D.; Laursen, K.; Yean Ong, W.; Yao, K.; Hwa Tay, J. Kinetic Study of Hydrated Lime Reaction with HCl. *Environ. Sci. Technol.* **2003**, 37, 2556-2562.
- (18) Koch, M.; Zhang, X.; Deng, J.; Kavouras, A.; Krammer, G.; Ge, L. Reaction mechanism of a single calcium hydroxide particle with humidified HCl. *Chem. Eng. Sci.* **2005**, 60, 5819-5829.
- (19) Duo, W.; Seville, J.P.K.; Kirkby, N.F.; Clift, R. Prediction of Dry Scrubbing Process Performance. In: Clift, R., Seville, J.P.K. (Ed.). *Gas Cleaning at High Temperatures*; Springer: Berlin (Germany), **1993**, pp. 644-662.